DEFENSE TECHNICAL INFORMATION CENTER

Information for the Defense Community

DTIC® has determined on 07/16/2010 that this Technical Document has the Distribution Statement checked below. The current distribution for this document can be found in the DTIC® Technical Report Database.

☒ **DISTRIBUTION STATEMENT A.** Approved for public release; distribution is unlimited.

☐ **© COPYRIGHTED**; U.S. Government or Federal Rights License. All other rights and uses except those permitted by copyright law are reserved by the copyright owner.

☐ **DISTRIBUTION STATEMENT B.** Distribution authorized to U.S. Government agencies only (fill in reason) (date of determination). Other requests for this document shall be referred to (insert controlling DoD office)

☐ **DISTRIBUTION STATEMENT C.** Distribution authorized to U.S. Government Agencies and their contractors (fill in reason) (date of determination). Other requests for this document shall be referred to (insert controlling DoD office)

☐ **DISTRIBUTION STATEMENT D.** Distribution authorized to the Department of Defense and U.S. DoD contractors only (fill in reason) (date of determination). Other requests shall be referred to (insert controlling DoD office).

☐ **DISTRIBUTION STATEMENT E.** Distribution authorized to DoD Components only (fill in reason) (date of determination). Other requests shall be referred to (insert controlling DoD office).

☐ **DISTRIBUTION STATEMENT F.** Further dissemination only as directed by (inserting controlling DoD office) (date of determination) or higher DoD authority.

Distribution Statement F is also used when a document does not contain a distribution statement and no distribution statement can be determined.

☐ **DISTRIBUTION STATEMENT X.** Distribution authorized to U.S. Government Agencies and private individuals or enterprises eligible to obtain export-controlled technical data in accordance with DoDD 5230.25; (date of determination). DoD Controlling Office is (insert controlling DoD office).

Detection of 2-photon oxidation from a NIR laser using confocal microscopy

Kurt J. Schuster[1], Larry E. Estlack[3], Benjamin A. Rockwell[2], Michael L. Denton[1*]

[1]Northrop Grumman, 4241 Woodcock Dr., Ste B-100, San Antonio, TX 78228-1330
[2]U.S. Air Force AFRL/HEDO, Brooks City-Base, TX 78235-5278
[3]Conceptual Mindworks, Inc., 4318 Woodcock Dr., #210, San Antonio, TX 78228-1330

ABSTRACT

Recent studies have determined that photochemical oxidation in cultured cells can be detected at peak irradiances as low as 8.5×10^8 W cm^{-2} (87-fs pulse). Fluorescent dyes, such as CM-H_2DCFDA, enable us to quantify the oxidation response of cells to mode-locked near-infrared (NIR) laser exposure. Using a modified confocal microscope, we characterize the time-dependent 2-photon induced fluorescence generated from a given NIR laser exposure. When cultured cells were then pre-loaded with antioxidants, ascorbic acid or N-acetyl-L-cysteine (NAC), they inhibit nonlinear oxidation with different efficiencies, providing insight regarding mechanisms of damage.

Keywords: 2-photon excitation, modelocked, femtosecond, photo-oxidation, confocal microscope, inhibitor, antioxidant

1. INTRODUCTION

In many applications[1-7], near-infrared (NIR) modelocked lasers are preferred over continuous wave lasers for their characteristically high peak-power delivered in ultrashort pulses to produce nonlinear effects. These properties are used in a multitude of applications, which include multiphoton microscopy and spectroscopy. Other uses for modelocked femtosecond lasers include diagnosis[8-9] and treatment[10] in humans, where the laser provides an increased transmittance in biomaterials. These properties are also important for *in vivo* fluorescent imaging and tracking of circulating cells.

At very high peak-irradiances (E_P), ultrashort pulses can result in laser induced breakdown[11] and free-electron production[12]. These extreme damage mechanisms can be used in nanodissection[13], where carefully delivered laser exposures are used (while keeping the cell viable). Understanding biological damage is paramount for the generation of these nonlinear effects when limiting collateral damage is desired.

Here we suggest to scientific, medical, and laser safety communities some means of reducing the photochemical effects generated by ultrashort laser pulses. Applying various antioxidants and visualizing rates of reactions with our modified confocal microscope setup[14], we show a reduction in oxidation response.

* Email: Michael.denton.ctr@brooks.af.mil; Phone: 210.563.8396
†Opinions, interpretations, conclusions, and recommendations are those of the authors and are not necessarily endorsed by the United States Air Force

Optical Interactions with Tissue and Cells XVII, edited by Steven L. Jacques, William P. Roach, Proc. of SPIE Vol. 6084, 60841H, (2006) · 1605-7422/06/$15 · doi: 10.1117/12.644651

2. METHODS AND MATERIALS

2.1 Cell culture

The human retinal pigment epithelial cell line (hTERT-RPE1; ClonTech) was used in all laser exposure experiments. Cultures were maintained in DMEM/F12 medium (10% fetal calf serum) at 37 °C and 5% CO_2. Cells were seeded into 35-mm Petri dishes at 300,000 cells per dish for use in experiments. Hank's balanced salt solution (HBSS) was used whenever cells were rinsed, loaded with fluorescent dye and inhibitors, and when exposed to lasers. Temperature regulation (25-28 °C) at the Confocal Laser-Damage Imaging System (CL-DIS) was provided by heating an aluminium block containing a central hole for the 35-mm culture dish. The block was attached directly to the X-Y translation stage of the confocal microscope. The fluorescent dye dichlorodihydrofluorescein (CM-H_2DCFDA, Molecular Probes) was used to indicate production of intracellular reactive oxygen species (ROS). This occurs when CM-H_2DCFDA is converted to its oxidized form CM-DCF. Ascorbic acid (AA) (cat BP351-500, Fisher Scientific) or N-acetyl-L-cysteine (NAC) (cat A9165, Sigma-Aldrich) were co-loaded with the dye and acted to inhibit fluorescence; cells (preloaded with 25 μM CM-H_2DCFDA and varying concentrations of inhibitor) were incubated at 37 °C for 20 minutes prior to laser irradiation exposure.

2.2 Lasers and beam delivery

Modelocked (80 MHz) 810-nm output from a tunable Mai Tai Ti:sapphire laser (Spectra Physics) was attenuated (prior to pulse compensation) by the combination of a half-wave plate and polarizing cube. The laser beam was delivered to the cellular layer in the 35-mm culture dish using a 250-mm focal length lens and a 4-mm, right-angle prism suspended just below the objective. This arrangement of the microscope and the experimental laser beam delivery system is referred to as the CL-DIS and is shown in Figure 1. To correct for group velocity dispersion, a pulse compressor was constructed to minimize pulse duration at the sample. The corrected pulse duration of the modelocked exposure beam was 87 fs, as measured by GRENOUILLI (Swamp Optics), after passing through BK7 glass. The BK7 glass was used to approximate the group velocity dispersion that occurs in the glass (lens and prism) between the pulse compressor and exposure plane. The thickness of BK7 glass used is equivalent to the combined thickness of the focusing lens and prism in the CL-DIS. Beam power was measured at two locations; prior to the focusing lens and also after the prism. A power ratio between these two locations allowed power to be adjusted and set during the course of the experiment by following the power measured prior to the focusing lens. Beam spot size was determined by the knife-edge method[15]. This measurement was performed each day, in duplicate, prior to cell exposure.

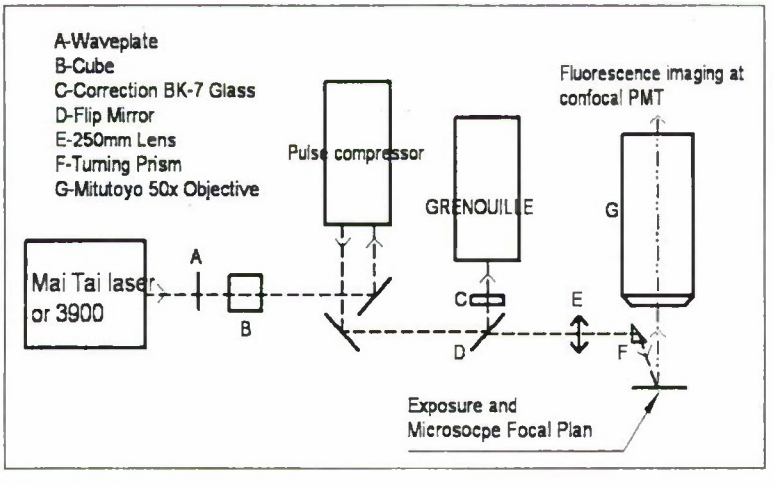

Figure 1: CL-DIS Setup. NIR laser radiation is emitted from the Mai Tai laser and incident upon a cube and waveplate combination for continuous power adjustment. The beam then travels through a pulse compressor and continues to the confocal microscope. A flip-up mirror is inserted into the path to direct a sample of the beam into a GRENOUILLE for accurate pulse duration measurement. A sample of glass is also placed between the flip-up and the GRENOUILLE to approximate the group velocity dispersion by the lens and prism.

2.3 Microscopy

Cells were visualized using a confocal laser-scanning microscope (Olympus BX61WI; Leeds Instruments, Inc, Irving, TX), fitted with a 50X objective (Mitutoyo Plan APO SL, Edmund Optics). For relative quantification of the oxidized CM-DCF fluorescence, acquisition parameters and settings on the microscope were the same for every exposure. Images were collected using FluoView 300 software with the automatic black-level adjustment deselected. For oxidation rate determination, cells were preloaded with CM-H_2DCFDA and exposed to varying irradiances of 3000, 6000, and 9000 W/cm^2. Separate dishes were then loaded with CM-H_2DCFDA/inhibitor and exposed to a constant 5,000 W cm^{-2} mean irradiance from the Mai Tai laser. Scanned confocal images were taken prior to, and at 10-s intervals during, the Mai Tai laser exposure, for a total exposure duration of 60 s.

Mean fluorescence was determined using FluoView 300 software. It was calculated using the total measured fluorescence units within a region of interest (ROI) and dividing by the number of pixels within the ROI. The ROI was defined as the laser spot size determined from the knife-edge measurement for that day. Measured laser-induced mean fluorescence was corrected by subtracting initial (t=0) fluorescence in the ROI and background fluorescence sampled outside the ROI at each subsequent time point.

2.4 Experimental Procedure

RPE cells, prepared for laser exposures as described in the Methods and Materials section, were brought into focus with the CL-DIS set-up. An external modelocked NIR beam was also focused to the same focal plane as the confocal microscope and directed to the center-of-view of the confocal microscope. This allowed for real-time data collection and analysis of oxidation fluorescence reactions. An external shutter controlled the exposure duration of the NIR beam while the scanning laser (488-nm wavelength) excited fluorescence, from the CM-DCF within the region of the NIR beam via single-photon excitation.

The 488-nm scanning laser from the confocal microscope is also an efficient photo-oxidant. To differentiate between NIR oxidation and scanning laser oxidation, postexposure images were analyzed using two different regions-of-interest. Average background fluorescence was calculated and subtracted from the average fluorescence induced by NIR radiation. This technique provided an accurate measurement of fluorescence produced by the scanning laser and allowed for background fluorescence subtraction.

3. RESULTS

3.1 2-Photon excitation oxidation

Figure 2 shows the oxidation fluorescence response with each time step (image panel). Following the progression of panels, one can visually qualify the very low background fluorescence generated by the 488-nm scanning laser. Oxidation fluorescence of CM-DCFDA often had a granular appearance around the nuclei of exposed cells. Fluorescence was seen to migrate throughout the cells during exposure. Each panel in Figure 2 shows an increasing oxidation response to the NIR modelocked laser indicated by intracellular fluorescence. Using FluoView 300 software, mean fluorescence can be quantified and corrected for background fluorescence.

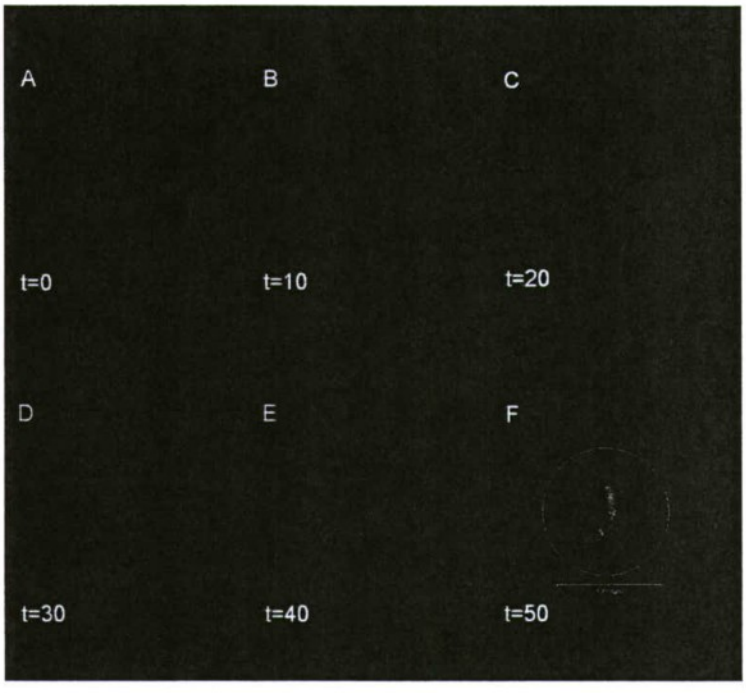

Figure 2: Time-lapse NIR Induced Photo-oxidation. Each panel shows a representative image of laser induced photo-oxidation at 10-s intervals. As time increases (left to right), the fluorescent intensity also increases. This is due to higher concentrations of ROS generated by the Mai Tai NIR modelocked laser. Shown in the last panel is the laser exposure spot size with scale bar (100 μm).

Figure 3 shows average corrected fluorescence with respect to laser exposure time. This graph shows that as time increases, the mean fluorescence also increases nonlinearly. This plot also shows that the intensity (in mean fluorescence) increases with an increasing mean irradiance. The oxidation response for 3000 W/cm^2 is near threshold and not as efficient as 6000 W/cm^2 or 9000 W/cm^2 mean irradiances.

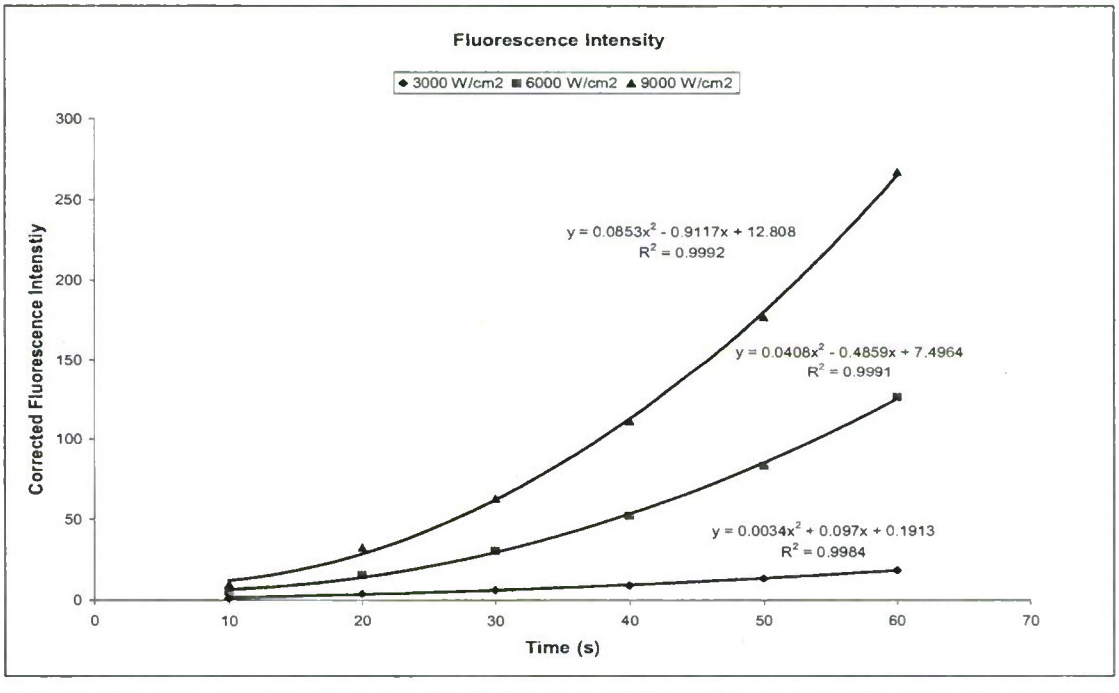

Figure 3: Time-dependent fluorescence showing the increase in oxidation (fluorescence) with respect to laser exposure (time). The oxidation dependence on laser irradiance is also apparent. ROS are more abundant with higher mean irradiances (9000 W/cm^2) than compared to lower irradiances (3000 W/cm^2).

When the oxidative fluorescence and irradiance data are plotted on log-log axes, the time points of the time-lapse data fell on a straight line[16,17]. Applying a linear regression through each time set yielded an average slope of 2.2 ± 0.22. The slopes of these lines indicate a power-squared dependence that supports the 2-photon excitation event.

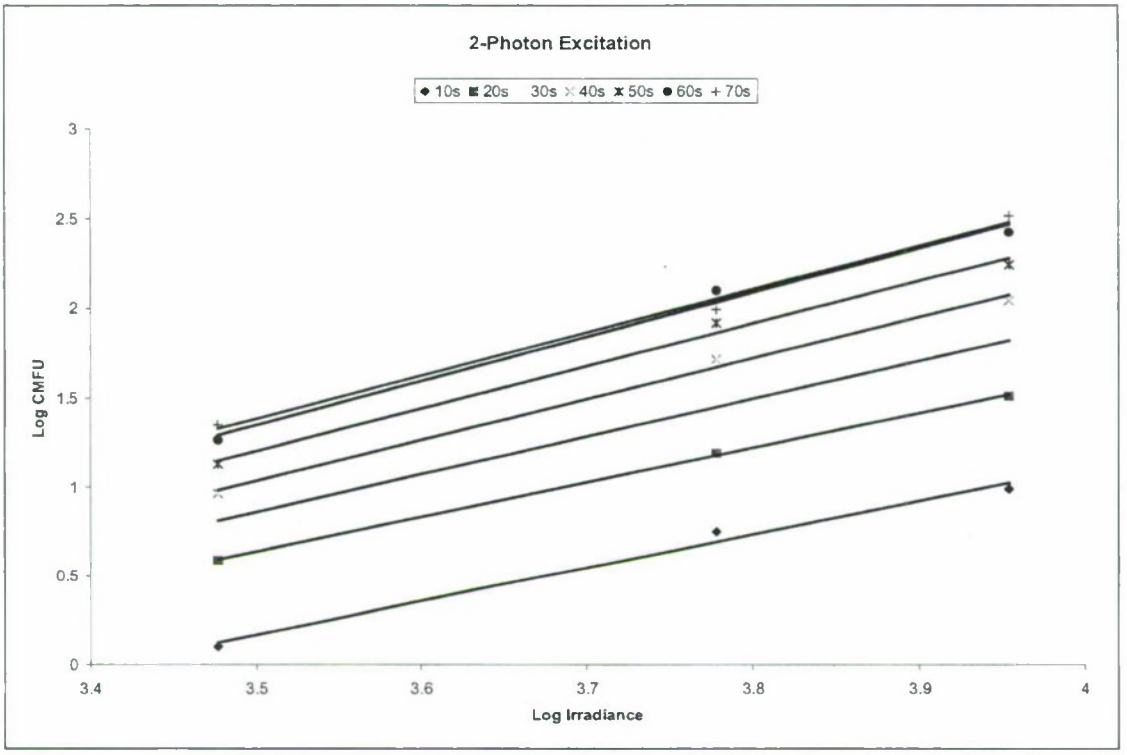

Figure 4: 2-Photon excitation: oxidation-irradiance from figure 2 is plotted on log-log axes. The average slope of each best-fit line is 2.2±0.22.

By fitting the fluorescence-time response data with a quadratic curve and calculating the second derivative, we can determine oxidation acceleration for each irradiance. Figure 4 shows the relationship between reaction acceleration and irradiance. Fitting these data with a linear function we can determine the minimum detectable mean irradiance. Using this method, we determine a minimum mean irradiance of 2960 W/cm^2 or threshold irradiance of 5920 W/cm^2 for a Gaussian beam. This corresponds with a peak irradiance (E_P) 8.5x10^8 W/cm^2.

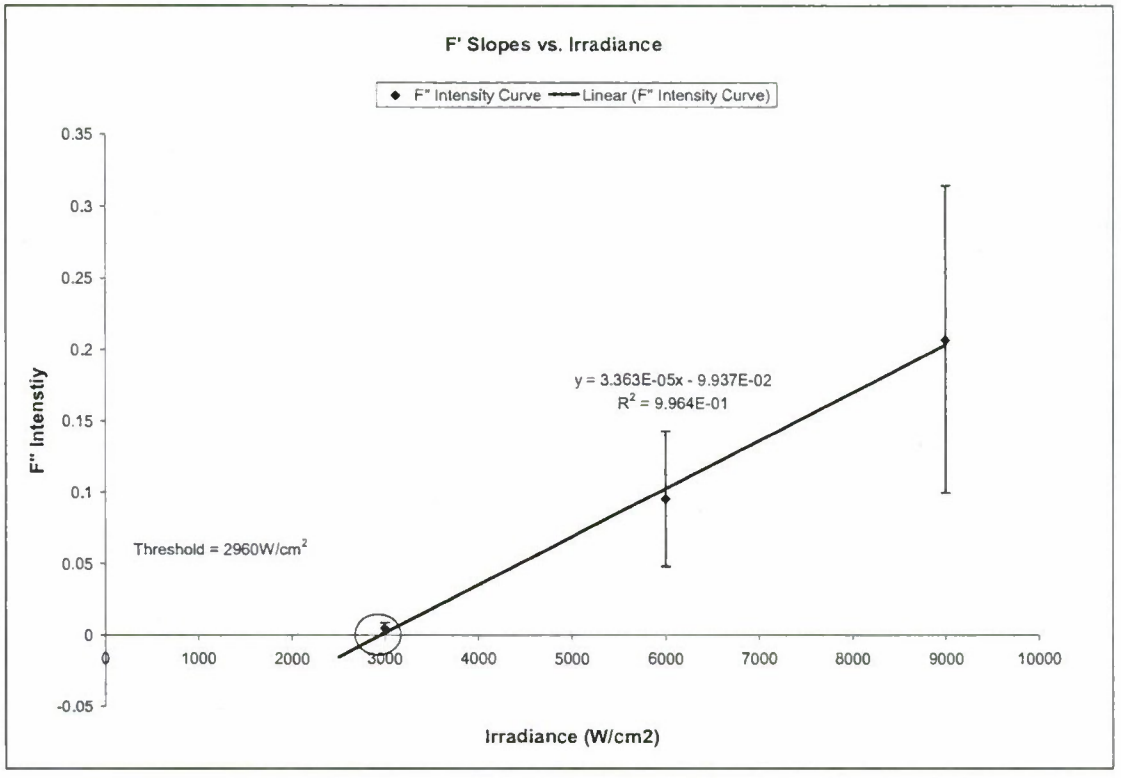

Figure 5: F″ vs. Irradiance. Plotting the calculated oxidation accelerations with their respective mean irradiance allows us to linearly extrapolate a threshold for oxidation reactions. Minimum irradiance for the oxidation, as calculated from the best fit line, is 2960 W/cm^2 mean irradiance.

3.2 Antioxidant Effects on 2-Photon Excitation Oxidation

RPE cells preloaded with CM-H_2DCFDA and varying concentrations of inhibitors (AA and NAC) were exposed to modelocked NIR radiation. The fluorescence-time response data were collected and analyzed, in the same manner as determining the threshold, by fitting the data with a quadratic curve and calculating the second derivative. The reaction acceleration calculated for each inhibitor concentration was then divided by the acceleration of the control (0 mM inhibitor). This allowed us to list the reaction accelerations as a fraction of the control.

Table 1 lists the fractional reduction of oxidation acceleration of cells loaded with AA. As the concentration of AA increases, the efficiency of the antioxidant increases. From these data, we see that ascorbic acid is an efficient antioxidant, where 0.25 mM concentrations decreases the oxidation acceleration by more than 60%, and even higher AA concentrations (2-3 mM) provided greater than 90% inhibition of oxidation. These data are also shown in Figure 5. Error was calculated as 1 standard deviation and is listed in Table 1 as percentage.

AA Concentration	Fractional Reduction of Oxidation	% Error
Control (0mM)	1	36
0.25 mM	0.38	18
0.5 mM	0.26	42
1 mM	0.18	36
2 mM	0.08	40
3 mM	0.09	56

Table 1: Ascorbic Acid Effects on 2-Photon Excitation

NAC Concentration	Fractional Reduction of Oxidation	% Error
Control (0 mM)	1	22
0.5 mM	0.97	17
2 mM	0.51	30
3 mM	0.64	25

Table 2: NAC Effects on 2-Photon Excitation

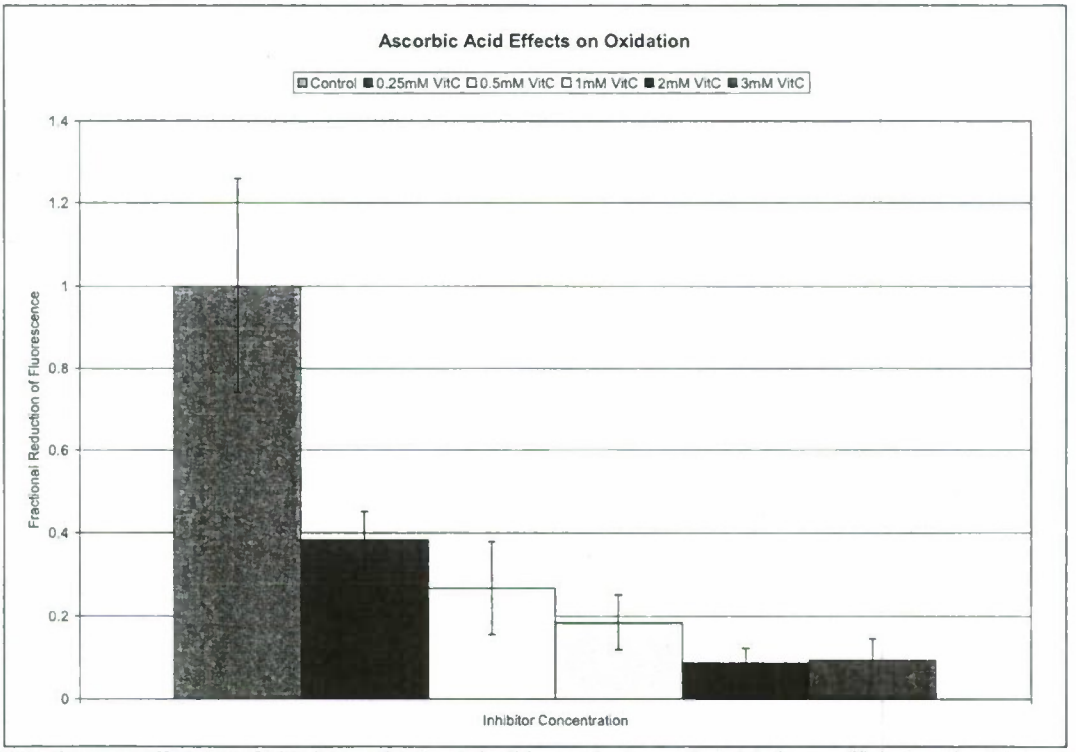

Figure 6: AA Effects on Oxidation. The trend in this graph shows that AA is an efficient antioxidant. AA concentrations of 2 mM provide nearly a 90% reduction of oxidation effects.

The fractional reduction of oxidation for NAC is listed in Table 2 and summarized in Figure 6. From these data it is shown that NAC does provide some antioxidant protection, with 2 mM concentrations reducing the oxidation rate by nearly half. However, ascorbic acid provides a far greater capacity of protection from our 2-photon excitation photo-oxidation.

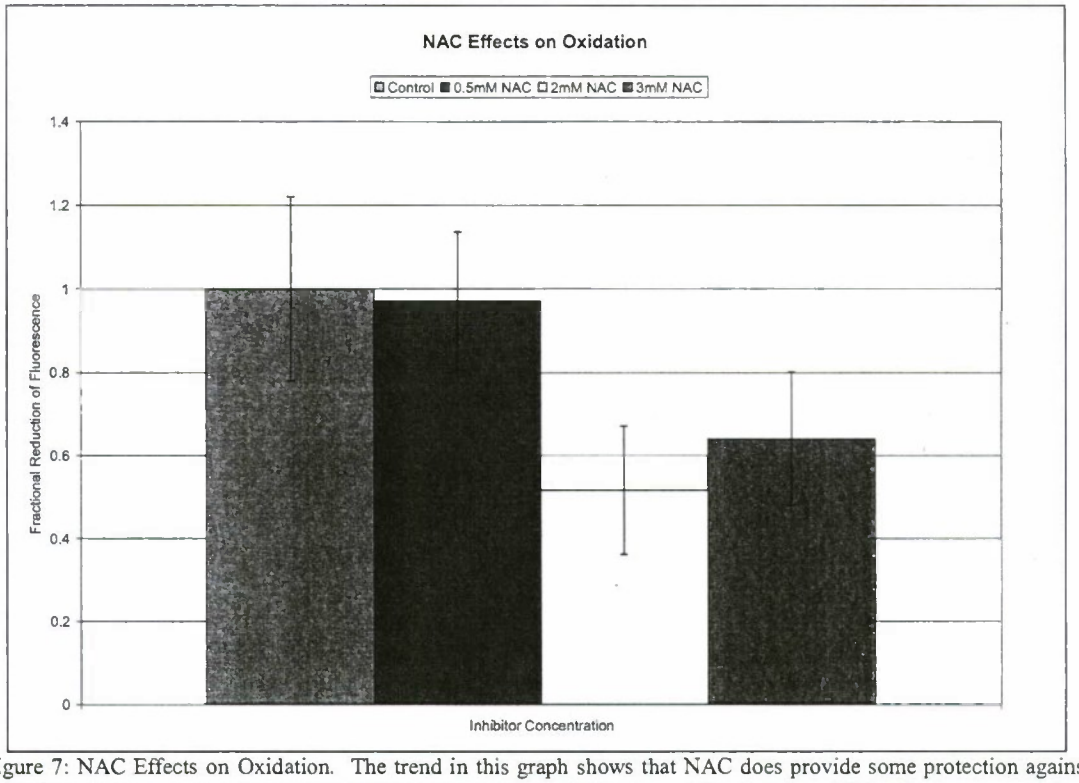

Figure 7: NAC Effects on Oxidation. The trend in this graph shows that NAC does provide some protection against oxidation. NAC is not as efficient as AA with similar concentrations providing less than 50% reduction in oxidation effects.

4. CONCLUSION

From the data collected and reported herein, we show that 2-photon events can occur at peak irradiance levels that are lower than previously thought possible. This also suggests that, with the aid of fluorescent dyes, ROS can be detected at these lower levels. Additionally, we report that AA and NAC both provide some protection from ROS. While both inhibitors provide protection, AA is more efficient at protecting cells from ROS than NAC. Our findings, though limited to two inhibitors, are significant with the treatment and prevention of photo-chemical laser induced damage.

REFERENCES

1 W. Denk. *et al.*, "Two-Photon Laser Scanning Fluorescence Microscopy", *Science*, **248**, 73-76 (year).

2 K. Berland, *et al.*, "Two-Photon fluorescence correlation spectroscopy: Method and application to the intracellular environment", *Biophys J* **68** 694-701 (year).

3 J. Bewersdorf, *et al.*, "Multifocal Multiphoton Microscopy", *Optic Letters* **12**, 655-657 (year).

4 E. Beaurepaire, *et al.*, "Combined Scanning Optical coherence and Two-Photon-Excited fluorescence Microscopy", *Optic Letters* **24**, 696-971 (year).

5 E. Sanchez, *et al.*, "Near-Field fluorescence Microscopy based on Two-Photon Excitation with Metal Tips", *Physical Review Letters* **82**, 4014-4017 (year).

6 J. Squirrell, *et al.*, "Long-Term Two-Photon Fluorescence Imaging of Mammilian Embryos Without compromising Viability" *Nat Biotechnol* **17** 763-767, (1999).

7 F. Helmchen, *et al.*, "A Miniature Head-Mounted Two-Photon Microscope: High-Resolution Brain Imaging in Freely Moving Animals" *Neuron*, **31**, 903-912, (2001).

8 B. Masters, *et al.*, "Multi-Photon Excitation Microscopy and Confocal Microscopy Imaging of in vivo Human Skin" *Microsc and Microanal* **5**, 282-289, (1999).

9 B. Masters, *et al.*, "Multi-Photon Excitation Microscopy of in vivo Human Skin. Funcitional and Morphological Optical Biopsy Based on Three Dimensional Imaging, Lifetime Measurements, and Fluorescence Spectroscopy", *Ann NY Acad Sci* **838,** (1998).

10 G. Maatz, "Chemical and Physical Side Effects at Applications of UltraShort Laser Pulses for Intrastromal Refractive Surgery", *J Opt. A.* **2**, 59-64, (2000).

11 P. Kennedy, "A First-Order Model for Computation of Laser-Induced Breakdown Thresholds in Ocular and Aqueous Media: Part 1-Theory", IEEE J. *Quantum electronics* **QE-31**, 2241, (1995).

12 B. Boudaiffa, "Resonant Formation of DNA Strand Breaks by Low-Energy Electrons", *Science* **287**, 1658-1660, (2000).

13 K. König, *et al.*, "Nanodissection of Human Chromosomes with Near-Infrared Femtosecond Laser pulses" *Optic Letters* **26**, 819-821, (2001).

14 M. Denton, *et al.*, "Accurate Measure of Laser Irradiance Threshold for NIR photo-oxidation with a modified confocal Microscope", *Journal of Microscopy*, In Press.

15 M. Schneider, W. Webb, "Measurement of submicron laser beam radii", *Applied Optics* **20**, 1382-1388, (1981).

16 C. Xu, W. Webb, "Measurement of Two-Photon Excitation Cross Section of Molecular Fluorophores with Data From 690 to 1050 nm", *J Opt Soc Am B* **13**, 481-491, (1996).

17 J. Lakokwicz, *et al.*, "Time-Resolved Fluorescence Spectroscopy and Imaging of DNA Labelled with DAPI and Hoechst 33342 Using Three-Photon Excitation", *Biophysical Journal* **72**, 567-578, (1997).